A measurement of the photon structure function F_2^γ at an average Q^2 of 12 GeV^2/c^4: results from DELPHI

P. Abreu, W. Adam, T. Adye, E. Agasi, I. Ajinenko, R. Aleksan, G D. Alekseev, P P. Allport, S. Almehed, S J. Alvsvaag, et al.

A measurement of the photon structure function F_2^γ at an average Q^2 of 12 GeV^2/c^4

DELPHI Collaboration

Abstract

The hadronic photon structure function F_2^γ has been measured in the Q^2 range from 4 to 30 GeV^2/c^4 and down to x values of order 0.001, using data taken with the DELPHI detector at LEP between 1991 and 1993. A comparison is made with several F_2^γ parameterizations with special emphasis on their low x behaviour. A result on the Q^2 evolution of F_2^γ is presented.

P.Abreu[21], W.Adam[50], T.Adye[37], E.Agasi[31], I.Ajinenko[42], R.Aleksan[39], G.D.Alekseev[16], P.P.Allport[22], S.Almehed[24], S.J.Alvsvaag[4], U.Amaldi[9], S.Amato[47], A.Andreazza[28], M.L.Andrieux[14], P.Antilogus[25], W-D.Apel[17], Y.Arnoud[39], B.Åsman[44], J-E.Augustin[19], A.Augustinus[31], P.Baillon[9], P.Bambade[19], F.Barao[21], R.Barate[14], D.Y.Bardin[16], G.J.Barker[35], A.Baroncelli[40], O.Barring[24], J.A.Barrio[26], W.Bartl[50], M.J.Bates[37], M.Battaglia[15], B.Batyunya[16], M.Baubillier[23], J.Baudot[39], K-H.Becks[52], M.Begalli[6], P.Beilliere[8], Yu.Belokopytov[9], K.Belous[42], A.C.Benvenuti[5], M.Berggren[47], D.Bertrand[2], F.Bianchi[45], M.Bigi[45], M.S.Bilenky[16], P.Billoir[23], D.Bloch[10], M.Blume[52], S.Blyth[35], V.Bocci[38], T.Bolognese[39], M.Bonesini[28], W.Bonivento[28], P.S.L.Booth[22], G.Borisov[42], C.Bosio[40], S.Bosworth[35], O.Botner[48], B.Bouquet[19], C.Bourdarios[9], T.J.V.Bowcock[22], M.Bozzo[13], P.Branchini[40], K.D.Brand[36], T.Brenke[52], R.A.Brenner[15], C.Bricman[2], L.Brillault[23], R.C.A.Brown[9], P.Bruckman[18], J-M.Brunet[8], L.Bugge[33], T.Buran[33], T.Burgsmueller[52], P.Buschmann[52], A.Buys[9], M.Caccia[28], M.Calvi[28], A.J.Camacho Rozas[41], T.Camporesi[9], V.Canale[38], M.Canepa[13], K.Cankocak[44], F.Cao[2], F.Carena[9], P.Carrilho[47], L.Carroll[22], C.Caso[13], M.V.Castillo Gimenez[49], A.Cattai[9], F.R.Cavallo[5], L.Cerrito[38], V.Chabaud[9], Ph.Charpentier[9], L.Chaussard[25], J.Chauveau[23], P.Checchia[36], G.A.Chelkov[16], R.Chierici[45], P.Chliapnikov[42], P.Chochula[7], V.Chorowicz[9], V.Cindro[43], P.Collins[9], J.L.Contreras[19], R.Contri[13], E.Cortina[49], G.Cosme[19], F.Cossutti[46], H.B.Crawley[1], D.Crennell[37], G.Crosetti[13], J.Cuevas Maestro[34], S.Czellar[15], E.Dahl-Jensen[29], J.Dahm[52], B.Dalmagne[19], M.Dam[33], G.Damgaard[29], A.Daum[17], P.D.Dauncey[37], M.Davenport[9], W.Da Silva[23], C.Defoix[8], G.Della Ricca[46], P.Delpierre[27], N.Demaria[35], A.De Angelis[9], H.De Boeck[2], W.De Boer[17], S.De Brabandere[2], C.De Clercq[2], C.De La Vaissiere[23], B.De Lotto[46], A.De Min[28], L.De Paula[47], C.De Saint-Jean[39], H.Dijkstra[9], L.Di Ciaccio[38], F.Djama[10], J.Dolbeau[8], M.Donszelmann[9], K.Doroba[51], M.Dracos[10], J.Drees[52], K.-A.Drees[52], M.Dris[32], Y.Dufour[8], F.Dupont[14], D.Edsall[1], R.Ehret[17], G.Eigen[4], T.Ekelof[48], G.Ekspong[44], M.Elsing[52], J-P.Engel[10], N.Ershaidat[23], B.Erzen[43], M.Espirito Santo[21], E.Falk[24], D.Fassouliotis[32], M.Feindt[9], A.Fenyuk[42], A.Ferrer[49], T.A.Filippas[32], A.Firestone[1], H.Foeth[9], E.Fokitis[32], F.Fontanelli[13], F.Formenti[9], B.Franek[37], P.Frenkiel[8], D.C.Fries[17], A.G.Frodesen[4], R.Fruhwirth[50], F.Fulda-Quenzer[19], H.Furstenau[9], J.Fuster[49], A.Galloni[22], D.Gamba[45], M.Gandelman[6], C.Garcia[49], J.Garcia[41], C.Gaspar[9], U.Gasparini[36], Ph.Gavillet[9], E.N.Gazis[32], D.Gele[10], J-P.Gerber[10], M.Gibbs[22], D.Gillespie[9], R.Gokieli[51], B.Golob[43], G.Gopal[37], L.Gorn[1], M.Gorski[51], Y.Gouz[42], V.Gracco[13], E.Graziani[40], G.Grosdidier[19], P.Gunnarsson[44], M.Gunther[48], J.Guy[37], U.Haedinger[17], F.Hahn[9], M.Hahn[17], S.Hahn[52], Z.Hajduk[18], A.Hallgren[48], K.Hamacher[52], W.Hao[31], F.J.Harris[35], V.Hedberg[24], J.J.Hernandez[49], P.Herquet[2], H.Herr[9], T.L.Hessing[9], E.Higon[49], H.J.Hilke[9], T.S.Hill[1], S-O.Holmgren[44], P.J.Holt[35], D.Holthuizen[31], M.Houlden[22], J.Hrubec[50], K.Huet[2], K.Hultqvist[44], P.Ioannou[3], J.N.Jackson[22], R.Jacobsson[44], P.Jalocha[18], R.Janik[7], G.Jarlskog[24], P.Jarry[39], B.Jean-Marie[19], E.K.Johansson[44], L.Jonsson[24], P.Jonsson[24], C.Joram[9], P.Juillot[10], M.Kaiser[17], G.Kalmus[37], F.Kapusta[23], M.Karlsson[44], E.Karvelas[11], S.Katsanevas[3], E.C.Katsoufis[32], R.Keranen[15], B.A.Khomenko[16], N.N.Khovanski[16], B.King[22], N.J.Kjaer[29], H.Klein[9], A.Klovning[4], P.Kluit[31], J.H.Koehne[17], B.Koene[31], P.Kokkinias[11], M.Koratzinos[9], K.Korcyl[18], V.Kostioukhine[42], C.Kourkoumelis[3], O.Kouznetsov[13], P.-H.Kramer[52], M.Krammer[50], C.Kreuter[17], J.Krolikowski[51], I.Kronkvist[24], Z.Krumstein[16], W.Krupinski[18], P.Kubinec[7], W.Kucewicz[18], K.Kurvinen[15], C.Lacasta[49], I.Laktineh[25], S.Lamblot[23], J.W.Lamsa[1], L.Lanceri[46], D.W.Lane[1], P.Langefeld[52], V.Lapin[42], I.Last[22], J-P.Laugier[39], R.Lauhakangas[15], G.Leder[50], F.Ledroit[14], V.Lefebure[2], C.K.Legan[1], R.Leitner[30], Y.Lemoigne[39], J.Lemonne[2], G.Lenzen[52], V.Lepeltier[19], T.Lesiak[36], D.Liko[50], R.Lindner[52], A.Lipniacka[19], I.Lippi[36], B.Loerstad[24], M.Lokajicek[12], J.G.Loken[35], J.M.Lopez[41], A.Lopez-Fernandez[9], M.A.Lopez Aguera[41], D.Loukas[11], P.Lutz[39], L.Lyons[35], J.MacNaughton[50], G.Maehlum[17], A.Maio[21], V.Malychev[16], F.Mandl[50], J.Marco[41], B.Marechal[47], M.Margoni[36], J-C.Marin[9], C.Mariotti[40], A.Markou[11], T.Maron[52], C.Martinez-Rivero[41], F.Martinez-Vidal[49], S.Marti i Garcia[49], F.Matorras[41], C.Matteuzzi[28], G.Matthiae[38], M.Mazzucato[36], M.Mc Cubbin[9], R.Mc Kay[1], R.Mc Nulty[22], J.Medbo[48], C.Meroni[28], W.T.Meyer[1], A.Miagkov[42], M.Michelotto[36], E.Migliore[45], L.Mirabito[25], U.Mjoernmark[24], T.Moa[44], R.Moeller[29], K.Moenig[9], M.R.Monge[13], P.Morettini[13], H.Mueller[17], L.M.Mundim[6], W.J.Murray[37], B.Muryn[18], G.Myatt[35], F.Naraghi[14], F.L.Navarria[5], S.Navas[49], P.Negri[28], S.Nemecek[12], W.Neumann[52], N.Neumeister[50], R.Nicolaidou[3], B.S.Nielsen[29], M.Nieuwenhuizen[31], V.Nikolaenko[10], P.Niss[44], A.Nomerotski[36], A.Normand[35], W.Oberschulte-Beckmann[17], V.Obraztsov[42], A.G.Olshevski[16], A.Onofre[21], R.Orava[15], K.Osterberg[15], A.Ouraou[39], P.Paganini[19], M.Paganoni[28], P.Pages[10], H.Palka[18], Th.D.Papadopoulou[32], L.Pape[9], C.Parkes[35], F.Parodi[13], A.Passeri[40], M.Pegoraro[36], L.Peralta[21], H.Pernegger[50], M.Pernicka[50], A.Perrotta[5], C.Petridou[46], A.Petrolini[13], H.T.Phillips[37], G.Piana[13], F.Pierre[39], M.Pimenta[21], S.Plaszczynski[19], O.Podobrin[17], M.E.Pol[6], G.Polok[18], P.Poropat[46], V.Pozdniakov[16], M.Prest[46], P.Privitera[38], N.Pukhaeva[16], A.Pullia[28], D.Radojicic[35], S.Ragazzi[28], H.Rahmani[32], J.Rames[12], P.N.Ratoff[20], A.L.Read[33], M.Reale[52], P.Rebecchi[19], N.G.Redaelli[28], M.Regler[50], D.Reid[9], P.B.Renton[35], L.K.Resvanis[3], F.Richard[19], J.Richardson[22], J.Ridky[12], G.Rinaudo[45], I.Ripp[39], A.Romero[45], I.Roncagliolo[13], P.Ronchese[36], L.Roos[14], E.I.Rosenberg[1], E.Rosso[9], P.Roudeau[19], T.Rovelli[5], W.Ruckstuhl[31], V.Ruhlmann-Kleider[39], A.Ruiz[41], K.Rybicki[18], H.Saarikko[15], Y.Sacquin[39], A.Sadovsky[16], G.Sajot[14], J.Salt[49], J.Sanchez[26], M.Sannino[13], H.Schneider[17], M.A.E.Schyns[52], G.Sciolla[45], F.Scuri[46], Y.Sedykh[16], A.M.Segar[35], A.Seitz[17], R.Sekulin[37], R.C.Shellard[6], I.Siccama[31], P.Siegrist[39], S.Simonetti[39], F.Simonetto[36], A.N.Sisakian[16], B.Sitar[7], T.B.Skaali[33], G.Smadja[25], N.Smirnov[42], O.Smirnova[16], G.R.Smith[37], R.Sosnowski[51], D.Souza-Santos[6], T.Spassov[21], E.Spiriti[40], P.Sponholz[52], S.Squarcia[13], C.Stanescu[40], S.Stapnes[33], I.Stavitski[36], K.Stepaniak[51], F.Stichelbaut[9], A.Stocchi[19], J.Strauss[50], R.Strub[10], B.Stugu[4], M.Szczekowski[51], M.Szeptycka[51], T.Tabarelli[28], J.P.Tavernet[23],

O.Tchikilev[42], A.Tilquin[27], J.Timmermans[31], L.G.Tkatchev[16], T.Todorov[10], D.Z.Toet[31], A.Tomaradze[2], B.Tome[21], L.Tortora[40], G.Transtromer[24], D.Treille[9], W.Trischuk[9], G.Tristram[8], A.Trombini[19], C.Troncon[28], A.Tsirou[9], M-L.Turluer[39], I.A.Tyapkin[16], M.Tyndel[37], S.Tzamarias[22], B.Ueberschaer[52], O.Ullaland[9], V.Uvarov[42], G.Valenti[5], E.Vallazza[9], C.Vander Velde[2], G.W.Van Apeldoorn[31], P.Van Dam[31], W.K.Van Doninck[2], J.Van Eldik[31], N.Vassilopoulos[35], G.Vegni[28], L.Ventura[36], W.Venus[37], F.Verbeure[2], M.Verlato[36], L.S.Vertogradov[16], D.Vilanova[39], P.Vincent[25], L.Vitale[46], E.Vlasov[42], A.S.Vodopyanov[16], V.Vrba[12], H.Wahlen[52], C.Walck[44], F.Waldner[46], M.Weierstall[52], P.Weilhammer[9], A.M.Wetherell[9], D.Wicke[52], J.H.Wickens[2], M.Wielers[17], G.R.Wilkinson[35], W.S.C.Williams[35], M.Winter[10], M.Witek[9], K.Woschnagg[48], K.Yip[35], O.Yushchenko[42], F.Zach[25], C.Zacharatou[24], A.Zalewska[18], P.Zalewski[51], D.Zavrtanik[43], E.Zevgolatakos[11], N.I.Zimin[16], M.Zito[39], D.Zontar[43], R.Zuberi[35], G.C.Zucchelli[44], G.Zumerle[36]

[1] Ames Laboratory and Department of Physics, Iowa State University, Ames IA 50011, USA
[2] Physics Department, Univ. Instelling Antwerpen, Universiteitsplein 1, B-2610 Wilrijk, Belgium
and IIHE, ULB-VUB, Pleinlaan 2, B-1050 Brussels, Belgium
and Faculté des Sciences, Univ. de l'Etat Mons, Av. Maistriau 19, B-7000 Mons, Belgium
[3] Physics Laboratory, University of Athens, Solonos Str. 104, GR-10680 Athens, Greece
[4] Department of Physics, University of Bergen, Allégaten 55, N-5007 Bergen, Norway
[5] Dipartimento di Fisica, Università di Bologna and INFN, Via Irnerio 46, I-40126 Bologna, Italy
[6] Centro Brasileiro de Pesquisas Físicas, rua Xavier Sigaud 150, RJ-22290 Rio de Janeiro, Brazil
and Depto. de Física, Pont. Univ. Católica, C.P. 38071 RJ-22453 Rio de Janeiro, Brazil
and Inst. de Física, Univ. Estadual do Rio de Janeiro, rua São Francisco Xavier 524, Rio de Janeiro, Brazil
[7] Comenius University, Faculty of Mathematics and Physics, Mlynska Dolina, SK-84215 Bratislava, Slovakia
[8] Collège de France, Lab. de Physique Corpusculaire, IN2P3-CNRS, F-75231 Paris Cedex 05, France
[9] CERN, CH-1211 Geneva 23, Switzerland
[10] Centre de Recherche Nucléaire, IN2P3 - CNRS/ULP - BP20, F-67037 Strasbourg Cedex, France
[11] Institute of Nuclear Physics, N.C.S.R. Demokritos, P.O. Box 60228, GR-15310 Athens, Greece
[12] FZU, Inst. of Physics of the C.A.S. High Energy Physics Division, Na Slovance 2, 180 40, Praha 8, Czech Republic
[13] Dipartimento di Fisica, Università di Genova and INFN, Via Dodecaneso 33, I-16146 Genova, Italy
[14] Institut des Sciences Nucléaires, IN2P3-CNRS, Université de Grenoble 1, F-38026 Grenoble Cedex, France
[15] Research Institute for High Energy Physics, SEFT, P.O. Box 9, FIN-00014 Helsinki, Finland
[16] Joint Institute for Nuclear Research, Dubna, Head Post Office, P.O. Box 79, 101 000 Moscow, Russian Federation
[17] Institut für Experimentelle Kernphysik, Universität Karlsruhe, Postfach 6980, D-76128 Karlsruhe, Germany
[18] High Energy Physics Laboratory, Institute of Nuclear Physics, Ul. Kawiory 26a, PL-30055 Krakow 30, Poland
[19] Université de Paris-Sud, Lab. de l'Accélérateur Linéaire, IN2P3-CNRS, Bât. 200, F-91405 Orsay Cedex, France
[20] School of Physics and Materials, University of Lancaster, Lancaster LA1 4YB, UK
[21] LIP, IST, FCUL - Av. Elias Garcia, 14-1°, P-1000 Lisboa Codex, Portugal
[22] Department of Physics, University of Liverpool, P.O. Box 147, Liverpool L69 3BX, UK
[23] LPNHE, IN2P3-CNRS, Universités Paris VI et VII, Tour 33 (RdC), 4 place Jussieu, F-75252 Paris Cedex 05, France
[24] Department of Physics, University of Lund, Sölvegatan 14, S-22363 Lund, Sweden
[25] Université Claude Bernard de Lyon, IPNL, IN2P3-CNRS, F-69622 Villeurbanne Cedex, France
[26] Universidad Complutense, Avda. Complutense s/n, E-28040 Madrid, Spain
[27] Univ. d'Aix - Marseille II - CPP, IN2P3-CNRS, F-13288 Marseille Cedex 09, France
[28] Dipartimento di Fisica, Università di Milano and INFN, Via Celoria 16, I-20133 Milan, Italy
[29] Niels Bohr Institute, Blegdamsvej 17, DK-2100 Copenhagen 0, Denmark
[30] NC, Nuclear Centre of MFF, Charles University, Areal MFF, V Holesovickach 2, 180 00, Praha 8, Czech Republic
[31] NIKHEF-H, Postbus 41882, NL-1009 DB Amsterdam, The Netherlands
[32] National Technical University, Physics Department, Zografou Campus, GR-15773 Athens, Greece
[33] Physics Department, University of Oslo, Blindern, N-1000 Oslo 3, Norway
[34] Dpto. Fisica, Univ. Oviedo, C/P. Pérez Casas, S/N-33006 Oviedo, Spain
[35] Department of Physics, University of Oxford, Keble Road, Oxford OX1 3RH, UK
[36] Dipartimento di Fisica, Università di Padova and INFN, Via Marzolo 8, I-35131 Padua, Italy
[37] Rutherford Appleton Laboratory, Chilton, Didcot OX11 OQX, UK
[38] Dipartimento di Fisica, Università di Roma II and INFN, Tor Vergata, I-00173 Rome, Italy
[39] Centre d'Etudes de Saclay, DSM/DAPNIA, F-91191 Gif-sur-Yvette Cedex, France
[40] Istituto Superiore di Sanità, Ist. Naz. di Fisica Nucl. (INFN), Viale Regina Elena 299, I-00161 Rome, Italy
[41] C.E.A.F.M., C.S.I.C. - Univ. Cantabria, Avda. los Castros, S/N-39006 Santander, Spain, (CICYT-AEN93-0832)
[42] Inst. for High Energy Physics, Serpukov P.O. Box 35, Protvino, (Moscow Region), Russian Federation
[43] J. Stefan Institute and Department of Physics, University of Ljubljana, Jamova 39, SI-61000 Ljubljana, Slovenia
[44] Fysikum, Stockholm University, Box 6730, S-113 85 Stockholm, Sweden
[45] Dipartimento di Fisica Sperimentale, Università di Torino and INFN, Via P. Giuria 1, I-10125 Turin, Italy
[46] Dipartimento di Fisica, Università di Trieste and INFN, Via A. Valerio 2, I-34127 Trieste, Italy
and Istituto di Fisica, Università di Udine, I-33100 Udine, Italy
[47] Univ. Federal do Rio de Janeiro, C.P. 68528 Cidade Univ., Ilha do Fundão BR-21945-970 Rio de Janeiro, Brazil
[48] Department of Radiation Sciences, University of Uppsala, P.O. Box 535, S-751 21 Uppsala, Sweden
[49] IFIC, Valencia-CSIC, and D.F.A.M.N., U. de Valencia, Avda. Dr. Moliner 50, E-46100 Burjassot (Valencia), Spain
[50] Institut für Hochenergiephysik, Österr. Akad. d. Wissensch., Nikolsdorfergasse 18, A-1050 Vienna, Austria
[51] Inst. Nuclear Studies and University of Warsaw, Ul. Hoza 69, PL-00681 Warsaw, Poland
[52] Fachbereich Physik, University of Wuppertal, Postfach 100 127, D-42097 Wuppertal 1, Germany

1 Introduction

In the reaction $e^+ e^- \rightarrow e^+ e^- X$, where X is a system of particles produced by the collision of two photons radiated from the beam particles, a scattered electron or positron can be detected (tagged). Measuring the electron[†] energy, E_{tag}, and the scattering angle, θ_{tag}, the squared momentum transfer of the corresponding photon is given by $-Q^2 = -4E_{tag}E_b \sin^2(\theta_{tag}/2)/c^2$, where E_b is the beam energy. In these so called "single tagged" events the other photon can be assumed to be almost on-shell, and the process is viewed as the deep inelastic scattering of the electron off the quasi-real target photon with a squared mass P^2 around zero (figure 1). The cross-section, expressed in terms of photon structure functions, is [1]:

$$\frac{d\sigma}{dxdy} = \frac{4\pi\alpha^2 s}{Q^4}\left[(1+(1-y)^2)F_2^\gamma(x,Q^2) - y^2 F_L^\gamma(x,Q^2)\right]N_\gamma(z,\theta_{max})zdz \qquad (1)$$

where

$$
\begin{aligned}
s &= 4E_b^2 \\
y &= 1 - (E_{tag}/E_b)\cos^2(\theta_{tag}/2) \\
x &= \frac{Q^2}{Q^2 + W_{\gamma\gamma}^2} \\
z &= \frac{E_\gamma}{E_b}
\end{aligned}
$$

$N_\gamma(z,\theta_{max})$ describes the flux of target photons with energy E_γ and θ_{max} is the maximum scattering angle of the undetected electron. $W_{\gamma\gamma}$ is the invariant mass of the $\gamma\gamma$ system. $F_2^\gamma(x,Q^2)$ and $F_L^\gamma(x,Q^2)$ are the photon structure functions.

Experimentally, since the scattered electron is tagged at relatively small angles and high energies ($<y> \simeq 0.1$), the measurement is only sensitive to $F_2^\gamma(x,Q^2)$. Neglecting y, the deep inelastic electron scattering off a quasi-real photon can be described through:

$$\frac{d\sigma(e\gamma \rightarrow eX)}{dxdQ^2} = \frac{4\pi\alpha^2}{Q^4}\frac{F_2^\gamma(x,Q^2)}{x} \qquad (2)$$

The QCD and QED photon structure functions are used depending on whether multi-hadronic or lepton pair final state is produced. The study of $F_2^{\gamma,QED}(x,Q^2)$, well known theoretically, allows the validity of the structure function formalism to be tested in the DELPHI experimental conditions and also permits the determination of the correct normalization for $F_2^{\gamma,QCD}(x,Q^2)$. The photon is known to couple to vector mesons (hadron-like behaviour), but the main interest in the study of $F_2^{\gamma,QCD}(x,Q^2)$ comes from the fact that the photon exhibits also a point-like coupling to the quarks. It has been predicted [2]

Fig.1

[†]In the following the term "electron" will be used for the tagged electron or positron.

that this coupling dominates the photon structure at large Q^2 (≥ 5 GeV$^2/c^4$) and large x. The $F_2^{\gamma,QCD}(x,Q^2)$ analysis also improves the understanding of the transition region between perturbative and non-perturbative regimes. Measurements of the photon structure function reported by previous experiments [3-8] have confirmed the existence of these two components.

An analysis of the QCD and QED photon structure functions[‡] using the data taken with the DELPHI detector at an average Q^2 of 12 GeV$^2/c^4$ is reported in the following.

2   Event selection and background estimate

A detailed description of the DELPHI detector can be found elsewhere [9]. Here only those aspects of the detector relevant to the present analysis are described.

The Small Angle Tagger (SAT) optimized for the luminosity measurement was used to tag the scattered electron. It covered the polar angles from 43 mrad to 135 mrad and consisted of alternating layers of lead sheets (0.9 mm thick) and plastic scintillating fibres (1 mm diameter) aligned parallel to the beam. The read-out segmentation was 8 rings in radius and 15°(7.5°) in azimuth for the inner (outer) 4 rings. The energy resolution of the SAT (σ/E) was 5.4% for an incident electron energy of 45 GeV and the angular resolution of the incoming electron was 1.9 mrad, thus giving an average resolution of the measured Q^2 to be about 10 %.

The selection of the single tagged events relied on the detection of the scattered electron in the SAT and the produced multihadronic or leptonic final state. The following criteria were used in order to select multihadronic events:

- The energy deposition in the SAT was required to be more than 30 GeV in one arm and less than 10 GeV in the other arm (the antitagging requirement). The choice of 30 GeV as a minimum for the energy of the tagged electron allowed the background to be reduced and the variable y to have a small average value.
- In addition to the lepton, at least three charged particles with momentum larger than 0.4 GeV/c were required. The charged particle polar angle θ was required to be between 20° and 160° in order to measure its momentum in the Time Projection Chamber (TPC) [9]. The relative error on the momentum was required to be less than 1, and the impact parameter smaller than 4 cm transverse to the beam axis and 10 cm along the beam axis.
- Neutral particles were accepted if they deposited at least 0.5 GeV in the Forward ElectroMagnetic Calorimeter (FEMC) and at least 1.0 GeV in the barrel one - High density Projection Chamber (HPC).
- The invariant mass of the hadron system was calculated using charged particles, assuming pion mass, and photons detected in HPC and FEMC. It was requested to range from 2 GeV/c^2 to 20 GeV/c^2. The lower limit was applied to avoid problems with the fragmentation reliability in the simulation and also to avoid the region of two-photon resonance production. The upper limit, together with the requirement on the total energy deposition to be lower than 15 GeV in the electromagnetic calorimeters, was used to remove background from Z^0 decays.
- The angle $\alpha_{R\phi}$ in the plane transverse to the beam axis between the tagged electron transverse momentum vector, $\vec{p}_T^{\,tag}$, and the vector sum of the hadrons transverse momenta, $\vec{p}_T^{\,had}$, was requested to be greater than 140°.

[‡]Most of the study was done for $F_2^{\gamma,QCD}(x,Q^2)$ and the subscript QCD will be omitted (or substituted by an acronym to emphasize the parameterization of F_2^γ used) in the following. The prefix QED will be pointed out explicitly.

The data collected during the period 1991 to 1993 at beam energies from 44.1 GeV to 47.5 GeV were processed. The data samples from different years have been shown to give compatible results, and they have been combined in the present analysis. The integrated luminosity was 60.6 pb^{-1}. After the selection 977 events were obtained. Remaining small backgrounds in the data sample are discussed below.

The squared mass of the virtual photon obtained from the measurement of the energy and polar angle of the tagged electron in the SAT varied from 4 GeV$^2/c^4$ to 30 GeV$^2/c^4$ with an average of 12 GeV$^2/c^4$.

The trigger study was based on the observation of a single charged particle in the forward and barrel regions [10]. The triggering efficiency for single tagged $\gamma\gamma$ events was found to be (95±1) %.

Using simulated $q\bar{q}$ and $\tau^+\tau^-$ pairs production from γ/Z^0 annihilation, the background from these processes was found to be negligible. The contribution from $\gamma\gamma \to \tau^+\tau^-$ with hadronic decay of the final $\tau^+(\tau^-)$ was estimated using simulated events produced with the TWOGAM generator [11]. The contamination was found to be 33±4 events (3.3% of the signal). The contribution from inelastic Compton events was evaluated using the program described in reference [12] and found to be negligible.

The background due to accidental coincidences of a signal in the SAT, coming from an off-momentum electron or a possible noise which faked a tagged electron, with a Z^0 or an untagged $\gamma\gamma$ event was estimated to be 1.5±0.5 events.

In order to determine the contamination from beam-gas events, the sidebands between 10 cm and 30 cm of the $|z|$ impact parameter distribution along the beam axis were used, assuming such events to be uniformly distributed along the z axis. The contamination from beam-gas events was estimated to be 5.5±1.8 events.

The estimated overall background (4 % of the signal) was not subtracted from the data sample.

3   Simulation and comparison with data

Previous experiments [3-8], which carried out the analysis of the two-photon interactions in the deep-inelastic regime, have demonstrated that a two component model, taking into account the duality of the behaviour of the target photon, satisfactorily describes the data.

The target photon can fluctuate into a bound state of $q\bar{q}$ (vector meson ρ, ω, ϕ ...) and the process looks like deep-inelastic electron-hadron scattering (hadron-like process). The description of such a process is non-perturbative. It was introduced through the Generalized Vector meson Dominance Model (GVDM) [13]. The multihadronic final system was generated as a $q\bar{q}$ system according to a distribution of the transverse momentum of the quark in the $\gamma\gamma$ center of mass system ($d\sigma/dp_T^2 \simeq \exp(-5p_T^2)$) and fragmented using JETSET 7.3 [14] with σ_q, the width of the Gaussian transverse momentum distribution for primary hadrons, taken to be 450 MeV/c [3].

On the other hand, the target photon can also split into quarks with a large transverse momentum with respect to the photon-photon axis (point-like component of the process). Here a perturbative calculation is available both in Quark Parton Model (QPM) [1] and QCD [15-17].

In the simulation of the predictions of the QPM model, the TWOGAM event generator was used with default parameters of the JETSET 7.3 program to fragment the produced quarks. The quark masses were taken to be 0.3 GeV/c^2 for u and d quarks, 0.5 GeV/c^2 for s and 1.6 GeV/c^2 for c quarks. Another event generator was used to describe QCD

corrections at the leading order, calculated in [17] based on the Field-Kapusta-Poggioli approach [15-16] (FKP parameterization) for light quark production. The cutoff parameter p_t^0 - the transverse momentum of the quark inside the target photon - was introduced into the FKP parameterization in order to separate the point-like and the hadron-like components. In practice, the meaningful parameter is the transverse squared mass, i.e. the sum of $(p_t^0)^2$ and the squared mass of a constituent quark, which is greater than the QCD scale parameter squared, Λ^2.

The generated events were passed through the detector simulation program [18] and then through the same event reconstruction program as for the real data.

The distributions of the charged multiplicity, the total momentum of the charged particles, the invariant mass of the hadronic system, the normalized energy of the tagged electron, Q^2 and $x_{visible}$ (computed using the tagged electron and the detected hadron system) for the data and the simulation are shown on figure 2. The dashed lines show the GVDM plus QPM predictions and have an expected number of events of 796±13. The GVDM plus FKP prediction for light quarks and QPM for heavy quark production, drawn by the dotted lines, have an expected number of events of 962±21 and satisfactorily describe the cross-section and the differential distributions as well. The GVDM and heavy quark contributions to the latter prediction were 339±7 and 135±3 events, respectively.

The shape difference between $F_2^{\gamma,FKP}$ and $F_2^{\gamma,QPM}$ (shown on figure 3) stems from the gluon radiation which shifts the x distribution to lower values. This gluon emission, which could affect the event topology, was not implemented in the event generator.

4 The unfolding

In order to obtain the photon structure function, the "detected" ("visible") x distribution must be unfolded to a "produced" ("true") one, since, due to the limited acceptance of the setup, many produced particles go undetected in and around the beam pipe and the "detected" invariant mass is systematically lower than the "produced" one. Using the simulation, it was found that, on average, 50 % of the "produced" invariant mass was detected in DELPHI. The energy resolution of the reconstructed particles had also to be taken into account, but it plays less role than the effect of the restricted detector acceptance.

The main features of the program used for the unfolding are given in the following, while the algorithm is described in detail in reference [19]. The simulation of events, generated with an input $F_2^{\gamma}(x)$ dependence, is used in order to get the correlation between the "true" and "visible" x values. The program treats x values of the data and the simulation through histograms. The unknown function $F_2^{\gamma}(x)$ is parameterized as a linear sum of spline functions multiplied by coefficients to be determined. The number of bins in the histograms and the number of splines are steering parameters to be defined by the user. For each simulated event the program determines a weight in order to reach the best fit to the $x_{visible}$ data distribution. The unfolded result of $F_2^{\gamma}(x)$ is then represented in the form of the histogram with the number of bins chosen to minimize their statistical correlations. The simulated events, weighted by the result of the unfolding, have then to reproduce data distributions which were not explicitly involved in the unfolding (control histograms). If, with the same $F_2^{\gamma}(x)$ dependence, the multihadronic final state was generated according to different models (including different behaviours of the quark transverse momentum), then the unfolding which corresponds to the best description of the control histograms is chosen.

Different tests of the program at the generator level were performed. One of them, which emphasizes the effect of the limited acceptance, is described here. An event sample, generated with a F_2^γ with slightly modified non leading terms, quoted as $F_2^{\gamma,FKP'}$ [15-17], was considered as a "data" sample and another sample generated with "unit" F_2^γ ($F_2^\gamma(x)/\alpha_{QED} \equiv 1$) was used to get the detector response (some criteria on the acceptance for the final state particles were applied at the generator level for both samples in order to simulate the experimental conditions). Figure 3 shows the result of the unfolding (only statistical errors, i.e. diagonal elements of a correlation matrix, are drawn) together with the input F_2^γ dependences. The curves reflect the effect of the target mass which will be discussed in the next section.

The events generated with "unit" F_2^γ were used for the unfolding of the data. In order to be consistent with the data, two multihadronic samples were simulated for the light quarks. The charm quark contamination, evaluated as 135 events, was treated as a background and was subtracted from the data according to the QPM prediction. The background (33 events) from $\gamma\gamma \to \tau^+\tau^-$ production was subtracted too. The first sample was generated with the point-like dependence for the transverse momentum of the produced quarks ($d\sigma/dp_T^2 \simeq p_T^{-4}$) in the $\gamma\gamma$ center of mass system, and the second one was generated with the hadron-like (limited p_T) dependence ($d\sigma/dp_T^2 \simeq \exp(-5p_T^2)$). The fragmentation of the produced quarks in each sample was done with the same parameters of JETSET 7.3 as was described above for each model.

5 $F_2^{\gamma,QED}$ and the effect of non-zero target mass

An additional test, which involves both the unfolding and the tagging method, is a study of the lepton pair production in the single tagged mode in order to obtain the known $F_2^{\gamma,QED}$. The muon pair production in the single tagged two photon interactions was studied. The events were selected if:

- There were only two charged particles with zero net charge and at least one of them had a hit in the muon chambers [9]. The minimum momentum was set to 1.5 GeV/c for one particle and 3 GeV/c for the other one. The charged particle polar angle, the error on the momentum and the requirements on the impact parameters were the same as for the hadron selection described above.
- The criteria on the tagged electron were the same as described in section 2.

The number of events selected was 619. The background from random coincidences in the SAT with untagged two-photon muon pair production was found to be lower than 2%. The background from tagged $\gamma\gamma \to \tau^+\tau^-$, evaluated using simulated events from the TWOGAM generator, was found to be below 2% and the contamination of radiative μ and τ pair production negligible. A satisfactory agreement of the data distributions with the simulation of the events generated by the TWOGAM generator was found. The predicted number of events was 615±19.

The simulation of the events generated with "unit" F_2^γ was used for the unfolding. This describes the effect of the finite resolution, since both produced muons were required to be detected and the "visible" and "produced" $\mu^+\mu^-$ invariant masses were equal within the error (2 %). Thus the effect of the Q^2 resolution (10 %) dominated this measurement.

The study of $F_2^{\gamma,QED}$ is an opportunity to test the model on the P^2 (squared mass of the target photon) dependence of the unfolded result (figure 4). Two approaches were used for the calculation of $F_2^{\gamma,QED}$ in order to compare it with the measured $F_2^{\gamma,QED}$. In the first approach the mean value of $F_2^{\gamma,QED}$ was calculated using a sample of P_i^2

derived from the simulation ($F_2 = < F_2(P_i^2) >$). The middle curve on figure 4 presents the result of the calculation. Another approach was the calculation using a fixed value of P^2 ($F_2 = F_2(P_{fixed}^2)$). The upper (lower) curve on figure 4 shows the calculation assuming a zero (mean) value for the target mass. The measurement is thus sensitive to the target mass. The calculation made under the assumption of zero target mass is systematically higher than the measured $F_2^{\gamma,QED}$. The mean value (0.13 GeV$^2/c^4$) of the target mass, obtained from the P_i^2 sample, gives a bad fit because of the non-Gaussian shape of the P^2 distribution. The fixed value of P^2, which gives a satisfactory fit to the measured $F_2^{\gamma,QED}$, was found to be around 0.04 GeV$^2/c^4$.

The same approaches were used for the $F_2^{\gamma,FKP}$ calculations. The three dotted curves on figure 3 have the same meaning as for $F_2^{\gamma,QED}$. The sensitivity of $F_2^{\gamma,FKP}$ to the target mass is weaker than that of $F_2^{\gamma,QED}$ since the use of the mean value of P^2 still gives a reasonable fit to the unfolded points.

The good agreement obtained with $F_2^{\gamma,QED}$ formalism indicates that the tagging method is understood well enough to be used for the QCD photon structure function measurement. The comparison with the theoretical expectations shows that the data is sensitive to the effect of the non-zero mass of the target photon and the model describes the P^2 behaviour properly.

In the following the first approach will be used for the $F_2^{\gamma,FKP}$ calculation in order to take into account the effect of the target mass. It should be noted however that the fixed value of P^2=0.04 GeV$^2/c^4$, being of the order of Λ^2, brings some theoretical uncertainties on the use of most of the parton density parameterizations given for the real photon. Nonetheless, these parameterizations will be used in the following, estimating these uncertainties to be at the 10 % level.

6 Parameterizations of the parton distribution in the photon

Various F_2^γ parameterizations have been developed for the light quarks [20-23]. In order to compare the "visible" distributions of the data with the events generated with the different $F_2^\gamma(x, Q^2)$ parameterizations, events were simulated with "unit" structure function and weighted. Each event was weighted as $F_2^\gamma(x_{true}, Q_{true}^2)$ in a given parameterization. Such a procedure allows any photon structure function parameterization to be used without additional production of simulated events.

Two invariant mass distributions[§] are compared in figure 5. The histogram presents the simulation of the events generated with the FKP formula inside the event generator while the simulation of the events generated with "unit" F_2^γ and then weighted is drawn by the crosses. The satisfactory agreement justifies of the approach described above.

The comparison of the invariant mass distribution of the data (the charm quark contribution was subtracted) with parameterizations suggested by Levy-Abramowicz-Charchula (LAC1) [20], Duke-Owens (DO) [22] (predicting a rise of F_2^γ at low values of x) and Gordon-Storrow (GS) [21] (without rise) is shown on figure 6. The hadron-like component was added to the models apart from the LAC1 model which includes it already. DO and GS parameterizations describe the data reasonably well, while the LAC1 one is far below. The rise at low x in the DO parameterization gives a small excess in the high invariant mass domain. The limited statistics do not allow a strong conclusion

---

[§]The invariant mass of the hadron system was chosen as the variable to be studied because the rise of F_2^γ at low x should give more events with a large invariant mass of the produced hadrons.

to be made based on the "visible" invariant mass distributions and the unfolding has to be used to convert the measurement of x into F_2^γ.

7 $F_2^{\gamma,QCD}$ and discussion

As mentioned above, the deep inelastic two-photon interaction is viewed as the interaction of the probe photon with the constituents of the target photon, coupling to a $q\bar{q}$ bound state (hadron-like part) or splitting into a free $q\bar{q}$ state (point-like part).

Theory predicts specific features for the behaviour of $F_2^\gamma(x, Q^2)$. The calculations have shown that the photon structure function increases with x. The Q^2 dependence of F_2^γ in the restricted x domain is found to be proportional to $\ln < Q^2 >$ [1]. Also, as discussed above, a rise at low x is predicted in some parameterizations of the parton content in the photon [20,22].

The experimental conditions for the present study, implied by the cuts imposed on the polar angle and energy of the tagged electron and by the minimal invariant mass required of the hadron system, limited the x domain to be unfolded up to 0.85. The lower limit of $x_{visible}$ (x_{true}) was of order 0.01 (0.001).

The systematic uncertainties due to the steering parameters dominate the result if the number of unfolded points is greater than four. In order to study the stability of the result of the unfolding, three different approaches were used in the simulation:

- Only the point-like events were used. The use of hadron-like events alone is known to give a false result since some simulated distributions (for instance, the high transverse momentum domain for the charged particles) are not populated enough to describe the data.
- The ratio of the number of point-like to hadron-like events used for the unfolding was set to the ratio predicted by the model.
- The hadron-like part was considered as a background, analogous to the charm quark contamination, and it was subtracted from the data according to the GVDM prediction. Then this prediction was added to the result of the unfolding for comparison with the above approaches.

The unfolded structure functions for the light quarks obtained under these three different approaches are shown on figure 7a by solid, dashed and dotted crosses respectively, according to their ordering in the above description. The measurement shows a satisfactory agreement. The upper (lower) curve on the figure shows the sum of the FKP prediction, calculated with Λ equal to 0.2 (0.3) GeV, and GVDM. It can be seen that the sensitivity of F_2^γ to Λ is weak.

Figure 8 shows the comparison of the control histograms of the data with the weighted simulation for the first two approaches. A small disagreement in the charged multiplicity indicates that more study is needed to tune the fragmentation of the produced quarks. Because the charged multiplicity was used to select the events, the disagreement affects the absolute normalization of the result. In order to estimate the magnitude of this effect, one more soft charged particle (with momentum below 0.6 GeV/c) was added to 10 % of the simulated events, providing a good agreement with the data in the charged multiplicity. The amount of data events rejected by the selection criteria (either with a charged multiplicity less or equal to 2 or with an invariant mass lower than 2 GeV/c^2) was then estimated to be lower than 4 %. This uncertainty in the absolute normalization was considered as a systematic error.

The FKP approach described above was chosen to present the final result since it gives a slightly better description of the control histograms (figure 8). The unfolded structure function for the light quarks at the average Q^2 of 12 GeV^2/c^4 is shown on figure 7b together with the measurement made by the OPAL experiment at an average Q^2 of 14.7 GeV^2/c^4 [8]. Two curves on the figure show the sum of the FKP prediction, calculated under different values of a phenomenological parameter p_t^0, and GVDM. The dotted (dashed-dotted) curve corresponds to the FKP calculation made with p_t^0 equal to zero (0.5) GeV/c. It is seen that the FKP parameterization is much more sensitive to the p_t^0 parameter than to the QCD scale parameter Λ (curves on figure 7a). The band on the lower part of figure 7b shows the effect of non-zero mass for the GVDM component. The upper (lower) edge of the band corresponds to the calculations made under zero (mean value of) target mass. The middle curve corresponds to the standard target mass in the GVDM calculation.

The following sources of systematic uncertainties were considered:

- The simulation of the detector and the effect of the fragmentation. The results are affected through the cuts applied to select the events. The selection criterion for the minimum charged multiplicity was changed to 4 and 5 and the analysis was repeated. The systematic error was calculated as a RMS variation of the result for each bin in x.
- The steering parameters for the unfolding. These parameters were varied and results with four unfolded points only were considered. The change in the result due to the variation of these parameters was then found to be within 10% to 35% of the statistical error of the result presented on figure 7.
- Others. A systematic uncertainty of 3 % was evaluated due to the c quark mass uncertainty (the mass was varied by ± 0.3 GeV/c^2 around the value used in the generation), an uncertainty of 2 % was estimated due to the effects of radiative correction (an event generator [24] including the radiative corrections was used), an uncertainty of 1 % from estimation of trigger efficiency and one of 4 % from the background calculation. The error due to the fixing of Q^2 at the average value was evaluated to be below 3 % by varying the Q^2 value used for the calculations at $\pm$ 20 % around the average value. The error due to the uncertainty in the luminosity measurement is negligible.

The numerical solution and the covariance matrix are presented in tables 1 and 2. A statistical test of the covariance matrix has shown that the correlations can be neglected to first order.

Table 1. Photon structure function

x bins	F_2^γ
0.001 - 0.080	0.21 $\pm$ 0.03(stat) $\pm$ 0.04(syst)
0.080 - 0.213	0.41 $\pm$ 0.04(stat) $\pm$ 0.05(syst)
0.213 - 0.428	0.45 $\pm$ 0.05(stat) $\pm$ 0.05(syst)
0.428 - 0.847	0.45 $\pm$ 0.11(stat) $\pm$ 0.10(syst)

Table 2. Correlation coefficients matrix

1st bin			
-0.33	2nd bin		
-0.10	-0.23	3rd bin	
0.06	-0.16	-0.27	4th bin

Figure 9 shows the Q^2 evolution of F_2^γ averaged for x between 0.3 and 0.8. Other measurements [3-8] are also presented for comparison. The low x limit was chosen in order to decrease the influence of hadron-like processes. The upper limit was set because of limited statistics in the large x region where it is difficult to get a stable result. The present result, adding the statistical and systematic errors in quadrature, is $F_2^\gamma(x)/\alpha_{QED}$=0.45±0.08 which is consistent with the QCD prediction.

An additional check of the F_2^γ behaviour in the low x domain has been made. In order to get more bins at low x, the data for $x_{visible}$ below 0.35 were unfolded. The result is shown on figure 10 together with various predictions. The numerical solution and the covariance matrix are presented in tables 3 and 4. Taking into account a 10% decrease of the predictions due to the non-zero target mass, GS and GRV parameterizations describe the measurement well. As an advantage of the unfolding procedure, the slight excess of DO parameterization over the data in the invariant mass distribution (figure 6) is now transformed into a large excess of the prediction over the unfolded result at low x. The LAC1 parameterization is in disagreement with the data. This conclusion could not be reached by the previous analysis in the untagged mode [25] since the jet production there gets contributions from both the quark an the gluon content of the photon.

Table 3. Photon structure function

x bins	F_2^γ
0.001 - 0.046	0.24 ± 0.03(stat) ± 0.05(syst)
0.046 - 0.117	0.41 ± 0.05(stat) ± 0.08(syst)
0.117 - 0.350	0.46 ± 0.17(stat) ± 0.09(syst)

Table 4. Correlation coefficients matrix

1st bin		
-0.33	2nd bin	
-0.10	-0.34	3rd bin

8 Conclusion

The QCD photon structure function F_2^γ has been measured at Q^2 from 4 GeV^2/c^4 to 30 GeV^2/c^4 with an average of 12 GeV^2/c^4. The result is consistent with the model prediction based on the QCD calculations. More study is needed to take into account the influence of gluon radiation on the fragmentation function. The measurement explores the x behaviour of $F_2^{\gamma,QCD}$ down to x of order 0.001 and no rise of the photon structure function in the small x domain has been found. GS and GRV parameterizations of the quark density in the photon are preferred over the LAC1 and DO ones. The result on the Q^2 evolution of $F_2^{\gamma,QCD}$ is consistent with QCD prediction. The QED photon structure function F_2^γ has also been measured and found in agreement with the theoretical expectation.

Acknowledgements

References

[1] V.M. Budnev *et. al.*, Phys. Rep. **15C** (1975) 181.

[2] C. Peterson, T.F. Walsh and P.M. Zerwas, Nucl. Phys. **B174** (1980) 424.

[3] H. Altoff *et. al.* (TASSO Collab.), Z. Phys. **C31** (1986) 527.

[4] W. Bartel *et. al.* (JADE Collab.), Z. Phys. **C24** (1984) 231.

[5] H. Aihara *et. al.* (TPC/2γ Collab.), Z. Phys. **C34** (1987) 1; Phys. Rev. Lett. **58** (1987) 97.

[6] Ch. Berger *et. al.* (PLUTO Collab.), Phys. Lett. **B149** (1984) 421; Nucl. Phys. **B281** (1987) 365.

[7] T. Sasaki *et. al.* (AMY Collab.), Phys. Lett. **B252** (1990) 491.

[8] P. Acton *et. al.* (OPAL Collab.), Z. Phys. **C61** (1994) 199.

[9] P. Aarnio *et. al.* (DELPHI Collab.), Nucl. Inst. Meth. **A303** (1991) 233.

[10] J.A. Fuster *et. al.*, DELPHI note 93-42 (1993), unpublished.

[11] S. Nova, A. Olshevski and T. Todorov,"A Monte Carlo event generator for two photon physics", DELPHI Note 90-35 (1990), unpublished.

[12] F.A. Berends, P.H. Daverveldt and R. Kleiss, Comp. Phys. Comm. **40** (1986) 285.

[13] J.J. Sakurai and D. Schildknecht, Phys. Lett. **B41** (1972) 489.

[14] T. Sjöstrand, Comp. Phys. Comm. **39** (1986) 347;
T. Sjöstrand and M. Bengtsson, Comp. Phys. Comm. **43** (1987) 367;
T. Sjöstrand, JETSET 7.3 manual, CERN-TH 6488/92 (1992).

[15] J.H. Field, F. Kapusta and L. Poggioli, Phys. Lett. **B181** (1986) 362.

[16] J.H. Field, F. Kapusta and L. Poggioli, Z. Phys. **C36** (1987) 121.

[17] F. Kapusta, Z. Physics **C42** (1989) 225.

[18] DELPHI collaboration, "DELPHI event generation and detector simulation - User guide", DELPHI Note 89-67 (1989), unpublished.

[19] V. Blobel, In Proceedings of the CERN School of Computing, Aiguablava, Spain (1984), CERN 85-09.

[20] H. Abramowicz, K. Charchula and A. Levy, Phys. Lett. **B269** (1991) 458.

[21] L.E.Gordon and J.K.Storrow, Z. Phys. **C56** (1992) 307.

[22] D.W.Duke and J.F.Owens, Phys. Rev. **D26** (1982) 1600.

[23] M. Glück, E. Reya and A. Vogt, Phys. Rev. **D45** (1992) 3986.

[24] F.A. Berends, P.H. Daverveldt and R. Kleiss, Comp. Phys. Comm. **40** (1986) 271.

[25] P. Abreu *et. al.* (DELPHI Collab.), Z. Phys. **C62** (1994) 357.
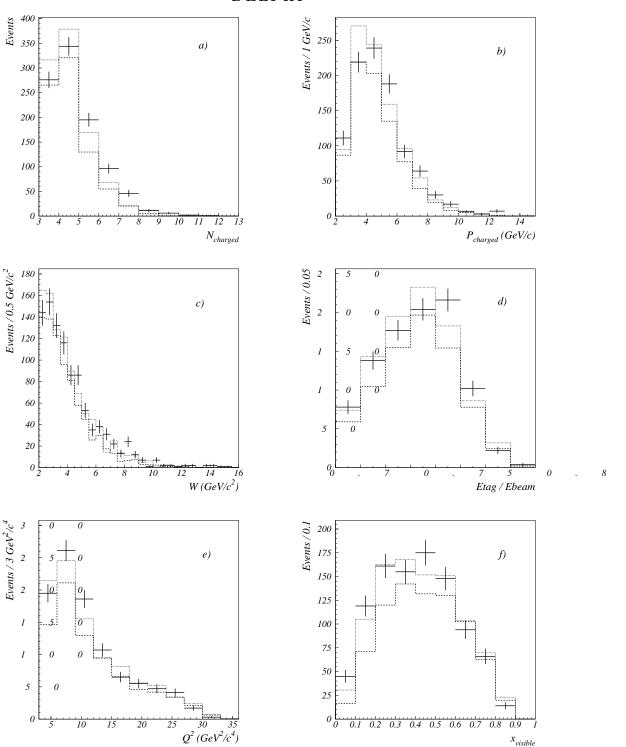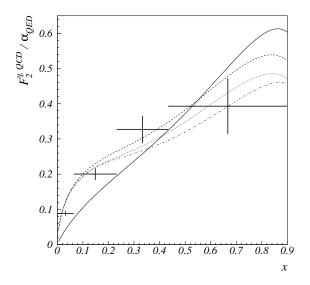
DELPHI

Fig.2 Comparison of the distributions for the data (crosses) and the simulation (histograms) for: (a) the charged multiplicity, (b) the scalar sum of the momenta of charged particles, (c) the invariant mass of the hadron system calculated using the charged particles and neutrals detected in the electromagnetic calorimeters, (d) the energy of the tagged electron normalized to the beam energy, (e) the squared momentum transfer Q^2 and (f) $x_{visible}$. The dashed lines show the QPM plus GVDM prediction, while the dotted lines show the prediction for the GVDM, QPM charm and FKP parameterization of the light quark density in the target photon.

Fig.3 Test of the unfolding of $F_2^{\gamma,FKP'}$ made at the generator level. The crosses are the unfolded result. The solid curve shows the $F_2^{\gamma,QPM}$ dependence while other curves show $F_2^{\gamma,FKP'}$, the input distribution calculated under different assumptions for the mass of the target photon, as discussed in the text.
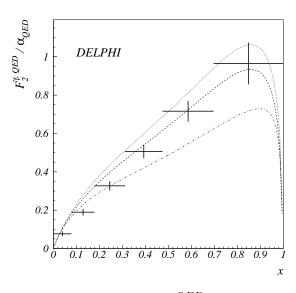
Fig.4 Unfolded $F_2^{\gamma,QED}$. The crosses are the unfolded result. The curves show $F_2^{\gamma,QED}$ calculated under different assumptions for the mass of the target photon: upper curve with zero mass, middle curve, using values from simulated data, lower curve taking the average value.
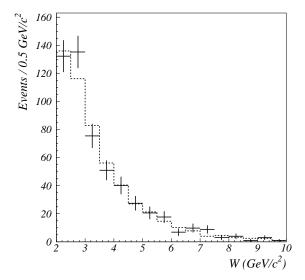

Fig.5 Invariant mass distributions for simulated events. The crosses show the distribution for the events generated with the $F_2^{\gamma,FKP}(x,Q^2)$ formula inside the event generator. The histogram presents the distribution of the events generated with "unit" F_2^{γ} and then weighted as $F_2^{\gamma,FKP}(x_{true},Q^2_{true})$ value for a given event.
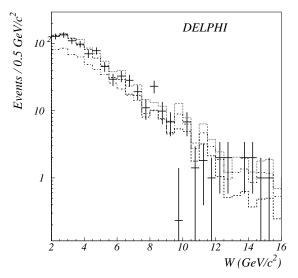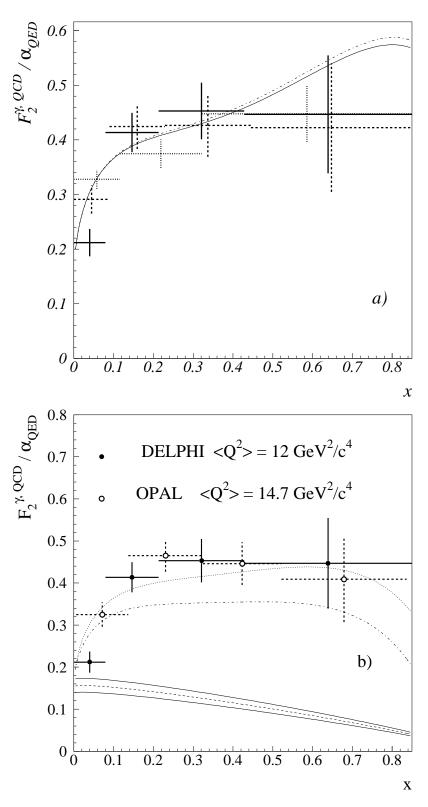
Fig.6 Comparison of the invariant mass distributions for the data drawn by the crosses and the simulation. The histograms show the predictions for GS [21] (dashed), DO [22] (dotted) and LAC1 [20] (dashed-dotted) parameterizations.

Fig.7 (a) Unfolded F_2^γ from light quarks simulated data for the different approaches drawn by the crosses and described in the text. The solid (dashed-dotted) curve presents the sum of the GVDM and FKP' prediction for the QCD scale parameter Λ equal to 0.3 GeV (0.2 GeV).

(b) Unfolded F_2^γ for light quarks at $< Q^2 > = 12$ GeV$^2/c^4$. The curves show the sum of the FKP prediction, calculated for values of $p_t^0 = 0.1$ GeV/c (upper curve) and 0.5 GeV/c (lower curve), and GVDM. The band, discussed in the text, shows the effect of the non-zero target mass for GVDM.
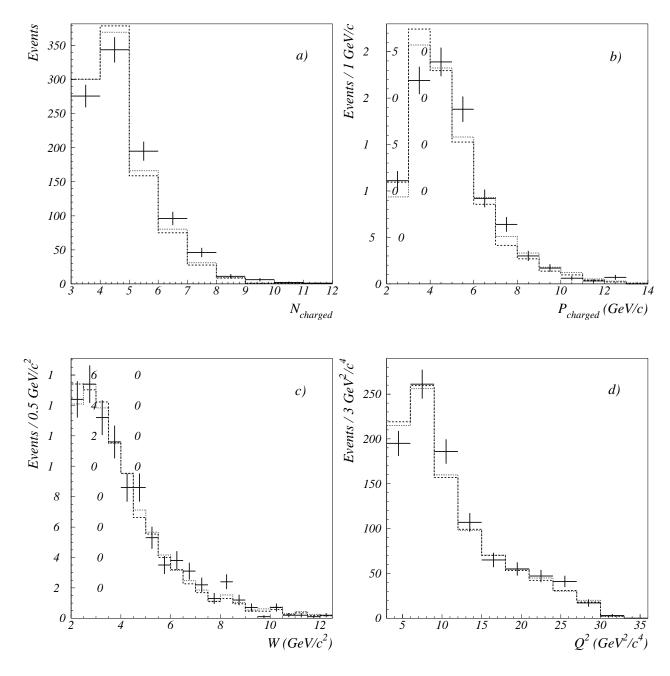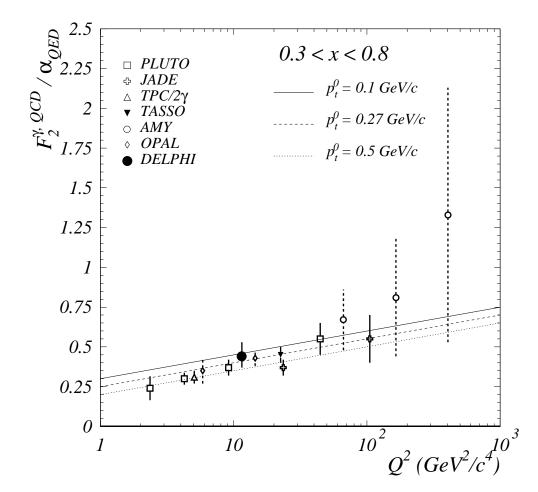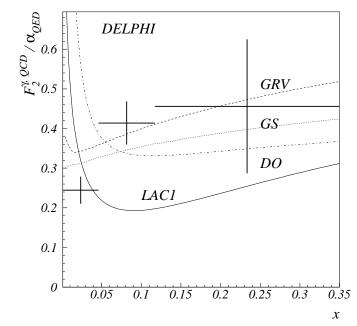
DELPHI

Fig.8 Comparison of the control histograms for the data and weighted simulated events for: (a) the charged multiplicity, (b) the total charged particle momentum, (c) the invariant mass of the hadron system and (d) the squared momentum transfer Q^2. The crosses present the data while two histograms show the result of the unfolding where the ratio of the number of the point-like events and the number of the hadron-like events used for the unfolding was set to the ratio predicted by the model (dashed) and where only the point-like events were used (dotted).

Fig.9 (adapted from [8]) Q^2 evolution of F_2^γ averaged between 0.3 and 0.8 of x. The lines show the QCD predictions with different phenomenological values of the cutoff parameter p_t^0 [15-17] - the transverse momentum of the quark inside the target photon.

Fig.10 Unfolded F_2^γ for $x_{visible}$ below 0.35. The curves show the LAC1 [20], GS [21], DO [22] and GRV [23] predictions.